

Structure and electrical levels of point defects in monoclinic zirconia

A. S. Foster,¹ V. B. Sulimov,² F. Lopez Gejo,² A. L. Shluger,² and R. M. Nieminen¹

¹Laboratory of Physics, Helsinki University of Technology, P.O. Box 1100, 02015, Finland

²Department of Physics and Astronomy, University College London, Gower Street, London WC1E 6BT, United Kingdom

(Received 2 July 2001; published 21 November 2001)

We performed plane wave density functional theory (DFT) calculations of formation energies, relaxed structures, and electrical levels of oxygen vacancies and interstitial oxygen atoms in monoclinic zirconia. The atomic structures of positively and negatively charged vacancies and interstitial oxygen atoms are also investigated. The ionization energies and electron affinities of interstitial oxygen atoms and oxygen vacancies in different charge states are calculated with respect to the bottom of the zirconia conduction band. Using the experimental band offset values at the interface of ZrO_2 films grown on silicon, we have found the positions of defect levels with respect to the bottom of silicon conduction band. The results demonstrate that interstitial oxygen atoms and positively charged oxygen vacancies can trap electrons from the bottom of the zirconia conduction band and from silicon. Neutral oxygen vacancy serves as a shallow hole trap for electrons injected from the silicon valence band. The calculations predict negative U for the O^- center and stability of V^+ centers with respect to disproportionation into V^{2+} and V^0 in monoclinic zirconia.

DOI: 10.1103/PhysRevB.64.224108

PACS number(s): 61.72.-y, 71.20.-b, 85.50.-n, 77.84.-s

I. INTRODUCTION

Zirconia is one of the most important wide band-gap transition metal oxides. Its current applications range from jewelry, semiconductor substrates, fuel cells and oxygen sensors to nuclear fuel rods.¹ Zirconia displays three polymorphs² at atmospheric pressure: at low temperatures the monoclinic C_{2h}^5 phase (space group $P2_1/c$), above 1400 K the tetragonal D_{4h}^{15} ($P4_2/nmc$) phase, and above 2600 K the cubic fluorite O_h^5 ($Fm\bar{3}m$) phase. Both the monoclinic and tetragonal phases can be obtained by distortion of the simple cubic structure. In general, at room temperature crystalline zirconia (ZrO_2) exists in the monoclinic phase, however, the cubic phase can be “stabilized” by the addition of substitutional cations, such as Ca^{2+} , Mg^{2+} , and Y^{3+} .¹ The stabilized zirconia has been extensively studied both theoretically and experimentally due to its wide technological applications.^{3,4} Recently, however, zirconia related research has received an additional boost due to an intensive search for new dielectric materials capable of substituting silicon dioxide in its role as gate dielectric in many microelectronic devices.⁵ Thin ZrO_2 films grown on silicon demonstrate favorable parameters, such as high thermal stability and low leakage current.^{6,7} High resolution TEM indicated the presence of both tetragonal and monoclinic phases in these films,⁷ and therefore studies of defect properties in these zirconia phases have become extremely topical.

The performance of thin zirconia films as gate dielectrics is likely to be affected by various defects. In particular, film growth involves oxygen diffusion through the already grown oxide and the possible formation of interstitial oxygen defects. Another important issue is related to oxygen stoichiometry and formation of oxygen vacancies. Electron and hole trapping by interstitial oxygen and oxygen vacancies may affect leakage current through the oxide. These issues are critical to the performance of thin zirconia films and have yet to be studied in tetragonal or monoclinic zirconia. Some

basic defect properties in cubic and cubic stabilized zirconia have been studied empirically,^{8,9} and using density functional theory.^{4,10} An extensive *ab-initio* investigation has also been performed for zircon (ZrSiO_4).¹¹

In this paper we present the results of the plane wave density functional theory (DFT) calculations of oxygen vacancies and interstitial oxygen atoms in monoclinic zirconia. After calculating the incorporation energies and structures of interstitial oxygen atoms and formation energies of neutral oxygen and zirconium vacancies, we consider the electron affinities and ionization energies of these defects and their structures in singly and doubly charged states. These properties are especially important at the interface with silicon as it may serve as an electron and hole source. The results demonstrate that interstitial oxygen atoms and positively charged oxygen vacancies can trap electrons from the bottom of the zirconia conduction band and from silicon.

The paper is organized as follows. In the next section we discuss the details and justification of the method of calculation. In the third section we discuss the results for the two classes of point defects, interstitials and vacancies, in the fourth section we study the energy levels of the defects, and then in the fifth section we discuss some possible reactions between defects. Finally, we summarize the implications and possible future directions of the study.

II. METHOD

All the calculations have been performed using the plane wave basis VASP code,^{12,13} implementing spin-polarized density function theory and the generalized gradient approximation (GGA) of Perdew and Wang¹⁴ known as GGA-II. We have used ultrasoft Vanderbilt pseudopotentials^{15,16} to represent the core electrons. The pseudopotential for the zirconium atom was generated in the electron configuration $[\text{Kr}]4d^35s^1$ and that for the oxygen atom in $[1s^2]2s^22p^4$, where the core electron configurations are shown in square brackets.

TABLE I. Comparison of calculated and experimental bulk unit cell parameters for the cubic, tetragonal, and monoclinic phases of zirconia. δz is the shift in fractional coordinates of oxygen atoms in the tetragonal cell with respect to their ideal cubic positions, β is the angle between lattice vectors a and c in the monoclinic cell and x, y, z are the fractional coordinates of the nonequivalent sites in the m structure.

Property	Calculated	Experimental ^a
	Cubic	
Volume (\AA^3)	32.97	32.97
a (\AA)	5.090	5.090
	Tetragonal	
Volume (\AA^3)	34.55	34.07
a (\AA)	3.628	3.571
c/a	1.447	1.451
δz	0.049	0.057
	Monoclinic	
Volume (\AA^3)	36.05	35.22
a (\AA)	5.192	5.150
b/a	1.014	1.012
c/a	1.032	1.032
β ($^\circ$)	99.81	99.23
x_{Zr}	0.277	0.275
y_{Zr}	0.044	0.040
z_{Zr}	0.209	0.208
x_{O_1}	0.072	0.070
y_{O_1}	0.338	0.332
z_{O_1}	0.341	0.345
x_{O_2}	0.447	0.450
y_{O_2}	0.758	0.757
z_{O_2}	0.479	0.479
	Energy differences between phases (/ZrO ₂)	
E^{t-c} (eV)	-0.07	-0.06
E^{m-c} (eV)	-0.17	-0.12

^aReferences 37 and 38.

In order to validate both the pseudopotentials and the method itself, extensive calculations were performed on the three dominant bulk phases of zirconia: cubic, tetragonal, and monoclinic. For each system, total energy convergence was tested within a k -point range between 1 and 60 k points and a plane wave cutoff energy range between 200 and 600 eV. Convergence to within 10 meV was achieved with 10 k points and a cutoff energy of 400 eV. The bulk unit cell lattice vectors and atomic coordinates were then relaxed at a series of fixed volumes. The obtained energies were fitted with a Murnaghan equation of state¹⁷ to give the equilibrium volume and the minimum energy. The final calculated cell parameters are given in Table I, along with experimental values. In all cases the agreement between calculated and experimental values is excellent, demonstrating that both the pseudopotentials and method are suitable for this study.

The electron density of states (DOS) for ideal monoclinic zirconia is shown in Fig. 1(a). For better presentation, each of the discrete one-electron energies forming the spectrum was broadened by a Gaussian with a smearing factor equal to

0.3 eV. Note that tails at the band edges are determined by this factor and do not have a quantitative meaning. The DOS for the monoclinic phase is very similar to the DOS obtained for the cubic and tetragonal phases (not shown here) and has three clear bands. A valence band of oxygen $2s$ character at around -15 eV, a valence band of oxygen $2p$ character at around 0 eV and a conduction band of zirconium $4d$ character at around 7 eV. There are a small number of states of Zr $4d$ character in the middle band, but it is dominated by the O $2p$ states. This is consistent with the picture of zirconia as an ionic insulator, with limited covalent bonding between Zr and O. The fact that the top of the Kohn-Sham O $2p$ valence band states is located at about 1.6 eV is determined by the pseudopotentials and by the way the Ewald summation is done in the code.

The band gap calculated as the energy difference between the highest occupied and lowest unoccupied one-electron states in this method is 3.41 eV. This energy is very close to that obtained in previous studies.¹⁸ Alternatively, it can be estimated as a difference of the total energies of the system with N , $N+1$, and $N-1$ electrons¹⁹

$$E_g(\text{theor}) = E(\text{per}, -1) + E(\text{per}, +1) - 2 \cdot E(\text{per}, 0). \quad (1)$$

Here $E(\text{per}, 0)$ is the total energy of the perfect neutral supercell, and $E(\text{per}, -1)$ and $E(\text{per}, +1)$ are the total energies of the supercell with an electron or a hole. In both charged states the electron and hole are completely delocalized over the supercell. A neutralizing background was applied to the unit cell for calculations of charged systems. The perfect crystal with an additional electron or hole becomes a metal and therefore calculations of its electronic structure may require a much larger number of k points than for a wide gap insulator. To investigate this issue we have calculated the energies $E(\text{per}, \pm 1)$ with four and ten k points and have found that the total energy changes only by about 0.003 eV. The band gap calculated in this way is equal to 3.19 eV. The gap values obtained using both methods are much smaller than the experimental values obtained by UPS [5.83 eV (Ref. 20)], EELS [4.2 eV (Ref. 21)] and electron photoinjection [5.4 eV (Ref. 22)]. The theoretical value calculated using the local density approximation in DFT and the perturbation theory on the GW level is equal to 5.4 eV.¹⁰

All defect calculations were made using a 96 atom unit cell, which is generated by extending the 12 atom monoclinic unit cell by two in all three dimensions. For this cell, the total energy was converged to better than 10 meV for a plane wave cutoff of 500 eV and 2 k points in the first Brillouin zone. One oxygen atom was added to or extracted from this cell to model the interstitial and vacancy defects, respectively. The large size of the cell separates the periodic defect images by over 10 \AA , greatly reducing the unphysical interactions between them. For geometry relaxation we used a combination of Conjugate Gradient energy minimization and quasi-Newton force minimization. During defect calculations the lattice vectors of the cell were frozen and all atoms were allowed to relax until atomic forces were less than 0.05 eV/ \AA . A neutralizing background was applied to the unit cell for calculations of charged defects. The Coulomb interaction

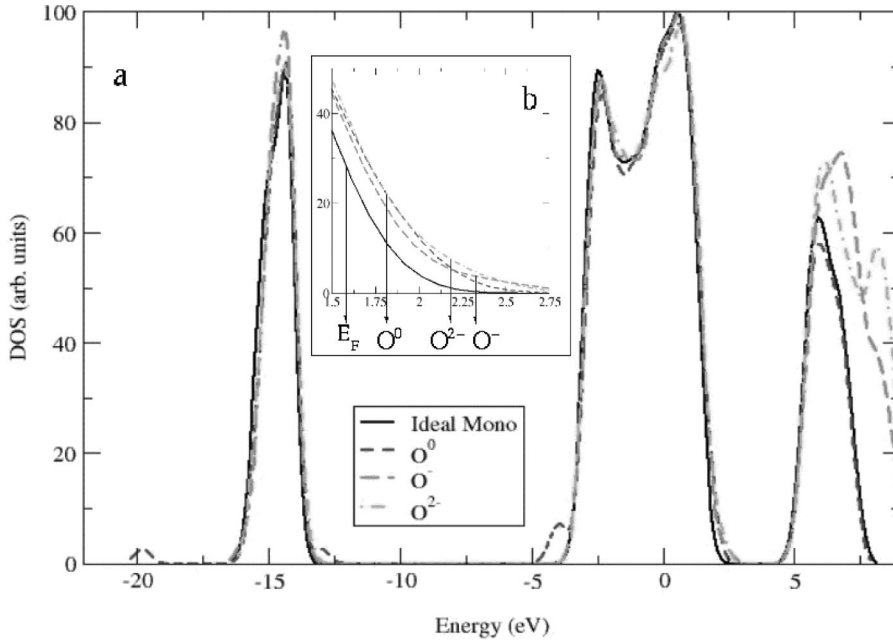


FIG. 1. (a) Total density of states (DOS) for ideal and defected monoclinic zirconia. Note that Gaussian smearing has been applied to the DOS for clarity. (b) A blow-up of the DOS around the Fermi level (E_F) of the ideal system, at 1.6 eV. The arrows show the one-electron positions of the defect states in the gap O^0 at 1.8 eV, O^{2-} at 2.2 eV, and O^- at 2.3 eV.

between charged defects in different periodic cells is calculated as described in Refs. 23,24 using Madelung constant as calculated in VASP.

The vacancy formation energies (or equivalently, the oxygen atom incorporation energies) $E_{\text{for}}(\text{defect})$ were calculated as the energy difference between the fully relaxed defected supercell $E(\text{defect})$ and the perfect monoclinic 96 atom unit cell $E(\text{per},0)$ and an isolated oxygen atom $E(O)$ according to

$$E_{\text{for}}(\text{defect}) = E(\text{defect}) - [E(\text{per}) \pm E(O)]. \quad (2)$$

Calculation of $E(O)$ presents some problems and is discussed in detail in the next section.

III. POINT DEFECTS

A. Oxygen interstitials

In this study we have considered defects formed by an interstitial oxygen atom in different charge states $X=O^0$, O^- , O^{2-} . As discussed below, each interstitial can form a stable defect pair with either a tetragonally (tetra) or triply bonded (triple) lattice oxygen (see Fig. 2). For ease of reference all values associated with a triply bonded oxygen will

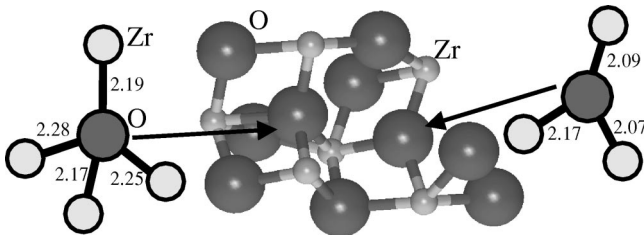


FIG. 2. Diagram showing the tetragonal (left) and triple-planar (right) bonding of the oxygen ions in the monoclinic phase of zirconia as calculated in this work. The numbers show interatomic distances in Å.

be labeled X_3 and all associated with a tetragonally bonded oxygen will be labeled X_4 , where X is the defect species.

The incorporation energy of atomic oxygen into zirconia lattice can be calculated with respect to different gas species. For example, an oxygen molecule in the lowest triplet state has been used in many similar studies (see, for example, Refs. 11,25,26). The reason for choosing this reference state is twofold: (i) molecular oxygen is used in some oxidation techniques and in this case provides the right reference for the chemical potential (see discussion in Ref. 11) and (ii) due to degeneracy of the ground triplet state of the oxygen atom, it is poorly described in DFT, especially in a periodic model. This degeneracy is lifted in the O_2 molecule, which provides a much better description. Using half of the energy of an isolated O_2 molecule (equal in our calculations to 4.91 eV) as a reference energy $E(O)$ [see Eq. (2)] we obtained the incorporation energies +1.4 eV for O_3^0 and +2.2 eV for O_4^0 . A positive value indicates an endothermic process, which involves dissociation of the O_2 molecule. However, to estimate whether the incorporation from atomic gas is exothermic, one should know the energy of an oxygen atom in the triplet state. This is known to be a problem in plane wave DFT as the result depends on the shape of the unit cell. Using a series of expanding rectangular periodic cells with three different lattice constants exceeding 10 Å, we obtained a “broken symmetry” solution for the oxygen atom with a lowest energy $E(O) = -1.97$ eV. This then gives the dissociation energy of the O_2 molecule in GGA-II as 5.88 eV, which is higher than the experimental value of 5.2 eV. The electron affinity of the oxygen atom calculated using the same approach is 1.7 eV, slightly higher than the experimental value of 1.46 eV.

Using the atomic $E(O)$ energy as a reference, we find that a single O atom is incorporated in the monoclinic zirconia lattice with an energy gain of -1.6 eV (O_3^0) and -0.8 eV (O_4^0). These values are close to those found for oxygen in-

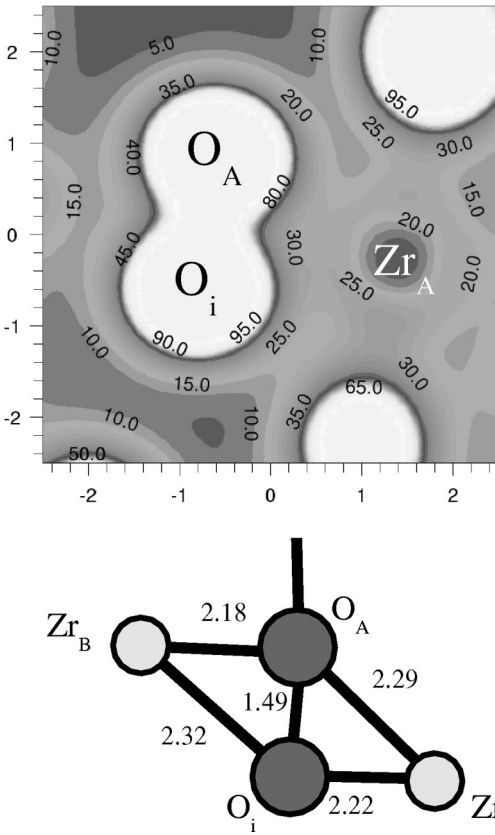


FIG. 3. Charge density in the plane through Zr_A , O_A and O_i , and a schematic diagram of neutral oxygen interstitial (O_i) near a triply bonded oxygen (O_A) in zirconia. Charge density is in $0.1 e/\text{\AA}$ and all distances are in \AA .

corporation in zircon.¹¹ They can be also compared with values reported in the literature for the same process in α quartz. Using a periodic LDA approach Hamann has found a formation energy of -0.86 eV,²⁷ a similar value -0.7 eV has been reported from correlated cluster calculations,²⁸ and -0.9 eV in recent DFT GGA-II calculations.^{25,26}

Figure 3 shows the fully relaxed charge density and position of ions near to a neutral oxygen interstitial in the (O_3^0) configuration in the lowest singlet state—the interstitial in the triplet state is 1 eV higher in energy. The charge density shows that the interstitial and lattice oxygen form a strong covalent bond, and effectively become a “dumbbell” defect pair within the lattice. This configuration is similar to previous calculations of neutral oxygen interstitials in zircon ($ZrSiO_4$),¹¹ but differs from the “peroxy bridge” seen in silica calculations.^{25,26} The lattice oxygen relaxes by up to 0.5 \AA to accommodate the interstitial, distorting the original triple planar O-Zr₃ group (see Fig. 2) into a slight pyramid with its apex pointing away from the interstitial. The Zr sublattice remains more or less undisturbed, with the nearest zirconium (Zr_A) to the pair only relaxing by around 0.05 \AA . Integration of the electron density around the oxygens within equivalent spheres of different radii using the LEV00 code²⁹ gives the same values for both the interstitial and the lattice oxygen, indicating that significant charge has been transferred to the interstitial.

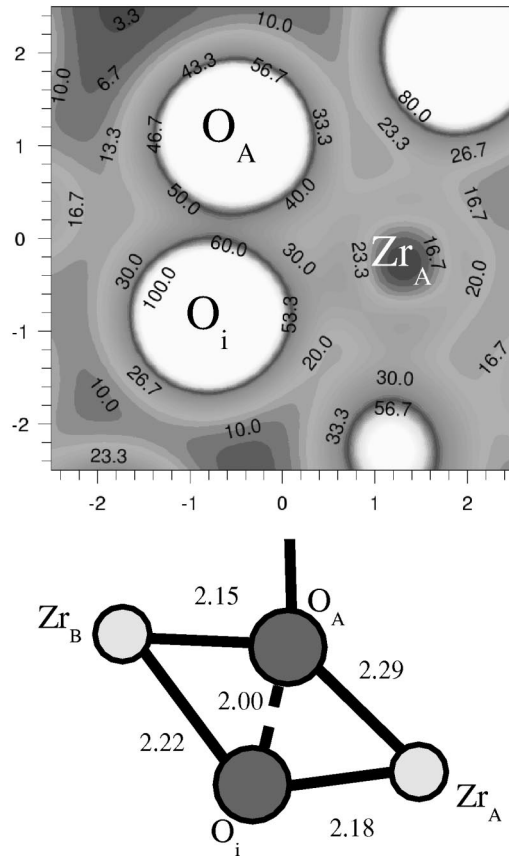


FIG. 4. Charge density in the plane through Zr_A , O_A , and O_i , and schematic diagram of singly charged oxygen interstitial (O_i) near a triply bonded oxygen (O_A) in zirconia. Charge density is in $0.1 e/\text{\AA}$ and all distances are in \AA .

To study the possibility of one and two electron trapping by the interstitial oxygen, we added extra electron(s) to the system. We should note that for both singly and doubly charged systems, the added electron initially went to the conduction band and did not localize fully on the defect until after the system was relaxed. Moreover, when we investigated the properties of the O_4^0 site, we found that when one or two extra electrons are added to this system, there is no stable energy minimum for the oxygen interstitial near to the tetragonal site. In fact the interstitial undergoes large displacements and moves to the most easily available triple oxygen site, forming an O_3^- defect. Due to this and since the triple oxygen site (O_3^0) in zirconia is energetically favored for interstitial formation, we will now focus in detail on defects incorporated at that site.

Figure 4 shows the charge density and positions of ions near to a singly negatively charged oxygen interstitial. The introduction of an extra electron causes the interstitial and lattice oxygen to separate, both displacing by about 0.2 \AA and also causing a 0.1 \AA displacement of the Zr_A . The relaxation energy from the initial O_3^0 configuration is equal to 1.7 eV. Overall this relaxation reduces the covalent bond between them significantly, as can be seen in the charge density plot. However, they remain effectively identical, with identical charge for a given radius. Calculation of the charge

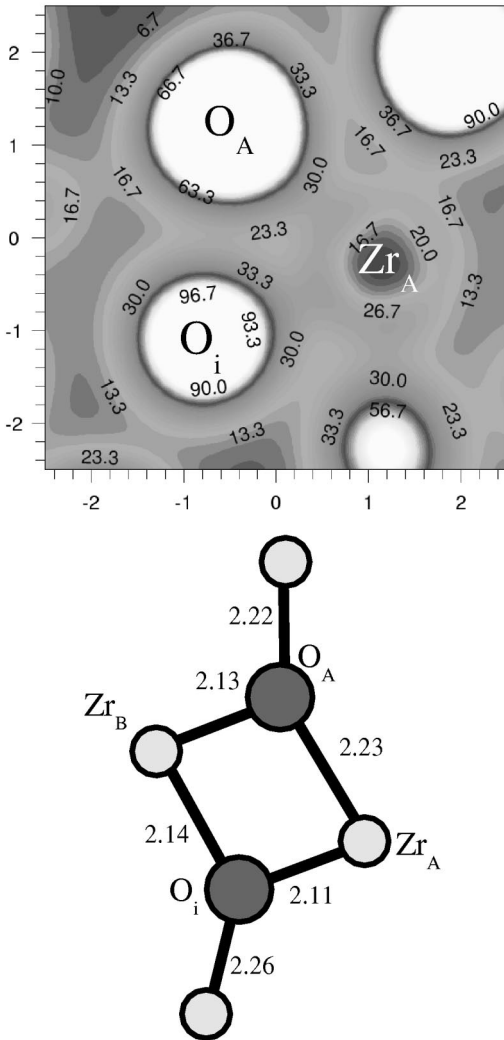


FIG. 5. Charge density in the plane through Zr_A , O_A , and O_i , and schematic diagram of doubly charged oxygen interstitial (O_i) near a triply bonded oxygen (O_A) in zirconia. Charge density is in $0.1 e/\text{\AA}$ and all distances are in \AA .

density difference between the system before and after the introduction of an electron shows that the electron is completely localized on the defect pair.

For the final interstitial, the doubly charged oxygen interstitial in Fig. 5, the charge density and positions differ significantly to that demonstrated for the singly charged defect. The interstitial displaces significantly (about 0.5\AA) to accommodate an extra electron and the corresponding relaxation energy is equal to about 1.4 eV . It now occupies an effective new triple site (see Fig. 5), bonding with a third zirconium ion. In the singly charged defect, the third zirconium ion was over 2.5\AA from the interstitial and no bond could be seen in the charge density. In this new configuration, the interstitial forms slightly elongated bonds with the zirconium ions compared to normal lattice triple site. The defect remains in the singlet state, with equal spin components. Again, calculation of the charge density difference between the systems before and after the introduction of the electron shows that the second electron is completely local-

ized on O_i and O_A . It also demonstrates a reduction of the covalent bond between O_i and the nearest zirconium ions.

The changing nature of the defect pair can also be seen in the evolution of the total density of states of the systems, shown in Fig. 1(a). On addition of the neutral oxygen interstitial, the main band structure remains the same, but new states can be seen. These are bonding and antibonding states of the O_i - O_A defect pair due to the extensive charge transfer and formation of a strong covalent bond. They are located at about -19 and -14 eV , and -4 and 1.8 eV , correspondingly. The highest occupied defect states are in the band gap near the top of the valence band at 1.8 eV . They are masked in the DOS tail and therefore indicated by the arrow in Fig. 1(b). For the singly charged oxygen interstitial, the O_i - O_A bond is weaker and the DOS is even closer to the ideal bulk DOS. The fact that the defect pair separates and becomes much more ionic means that there are now no other clear defect states in the DOS. Defect states which appear at the top of the valence band in the gap at about 2.3 eV are again indicated in Fig. 1(b). The DOS for the doubly charged interstitial is, again, very similar to that for the perfect lattice, with O_i^{2-} related defect states at about 2.2 eV in the gap.

We also studied the positive interstitial in zirconia, however, the hole does not localize on the defect even after relaxation. The charge density maps show that the hole is delocalized over the whole cell and the one-electron energy spectrum is typical for a metallic state. This may represent a well-known error in the kinetic energy calculated in Kohn-Sham theory, which favors delocalized over localized defect states³⁰ and can also be seen for the V_4^- defect below. Therefore this result may not be accurate and will not be discussed in detail.

B. Vacancies

In respect of two types of oxygen atoms in monoclinic zirconia we considered vacancies of fourfold and threefold coordinated oxygen: V_4 and V_3 . The main properties of both types of vacancies are very similar and the discussion below is presented in terms of fourfold coordinated vacancy V_4 .

We start our discussion from considering a neutral vacancy, which is formed by removing one neutral oxygen atom from the 96 atom unit cell. Formation of the neutral vacancy leads to a very small relaxation of the four neighboring Zr ions with displacements of only about 0.01 – 0.02\AA from their positions in the perfect crystal. The corresponding relaxation energy is $\sim 0.11 \text{ eV}$. The vacancy formation energy is defined as $E_{\text{for}}(V) = E(\text{vacancy}) + E(O) - E(\text{per},0)$, where $E(\text{vacancy})$ and $E(\text{per},0)$ are the supercell energy for the defective and the perfect systems, respectively, and $E(O) = -1.97 \text{ eV}$ is the energy of the free oxygen atom in the triplet state as used for the interstitial calculations. The formation energies for fourfold and threefold coordinated neutral oxygen vacancies are equal to $E_{\text{for}}(V_4) = 8.88 \text{ eV}$ and $E_{\text{for}}(V_3) = 8.90 \text{ eV}$, respectively. They are quite similar to those obtained for MgO and silica (see, for example, Refs. 31,32).

The neutral vacancy has a doubly occupied one-electron energy level deep in the forbidden gap and is strongly local-

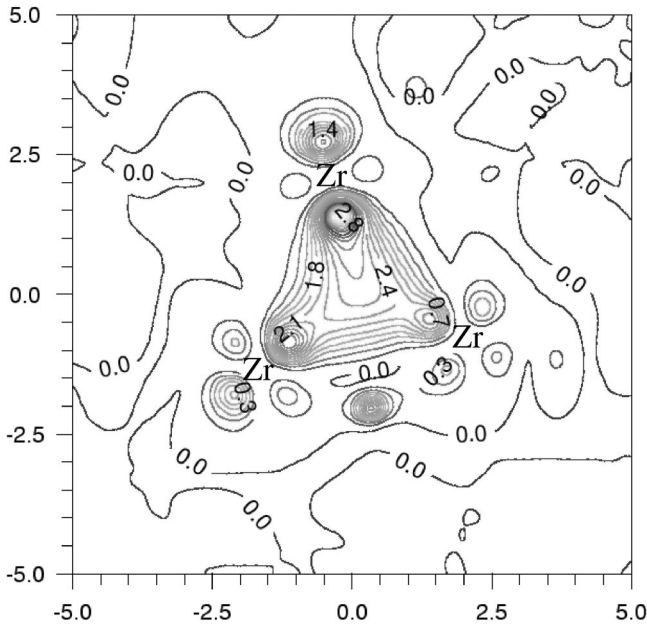


FIG. 6. Spin density map, in the plane through three Zr ions, of the positively charged vacancy V_4^+ . The vacancy position is at the center (0,0) of the map. Spin density is in $0.1 e/\text{\AA}$ and all distances are in \AA .

ized. This energy level is situated ~ 2.2 eV above the top of the valence band. The defect charge density distribution is qualitatively very similar to that for a neutral oxygen vacancy in cubic zirconia.¹⁰ It is strongly localized with a maximum in the center of the vacancy and can be described as a bonding combination of atomic orbitals of all four Zr neighboring the vacant site. The first one-electron excited state is situated very close to the conduction band edge and is much less localized with the charge density having maxima on all Zr ions beyond the first neighbors of the vacancy. The energy of the vertical (i.e., for the fixed geometry of the relaxed singlet state) singlet-to-triplet excitation (calculated as the difference of total energies of the defective supercell in the ground and excited triplet states) is equal to $E(S_0 \rightarrow T_1) = 1.2$ eV. We note that this value is very close to the energy difference between the corresponding occupied and unoccupied one-electron states.

Ionization of the neutral oxygen vacancy results in the creation of the positively charged defect V_4^+ . The spin density map presented in Fig. 6 clearly shows that the remaining electron is strongly localized in the vacancy. It also reflects the bonding character of the charge density corresponding to the singly occupied localized state and demonstrates strong contributions of Zr d orbitals. The atomic relaxation in this case is much stronger than for the neutral vacancy: all four Zr neighbors move away from the vacant site by about 0.1\AA and the relaxation energy amounts to 0.47 eV. Creation of the doubly positively charged vacancy V_4^{2+} is again accompanied by further displacement of the surrounding four Zr ions away from the vacant site by additional 0.1\AA . This leads to the further energy decrease by 0.74 eV.

We should note that strong localization of the electron density inside the vacancy and the behavior of the lattice

relaxation are qualitatively similar to that for neutral and charged oxygen vacancies in MgO (Ref. 31) and in alkali halide crystals.³³ Therefore these defects in zirconia can be attributed to the class of F centers.

There have been suggestions that negatively charged vacancies (F' centers³⁴) can also exist in zirconia. Therefore we considered trapping of an additional electron at the neutral oxygen vacancy V_4^0 and creation of the negatively charged vacancy V_4^- . In this charged state the additional electron is only weakly localized in the vicinity of the vacancy. The corresponding spin maps clearly show strong delocalization of the spin over the whole supercell. Therefore the atomic relaxation is very small: all four Zr neighbors displace by less than 0.02\AA and the energy decreases by less than 0.1 eV. The same conclusion can be made by analyzing the one-electron states which demonstrate a clearly metallic solution.

For completeness, we have also considered a neutral Zr vacancy. This corresponds to removing a neutral zirconium atom from a lattice site. The lattice relaxation in this case is significantly stronger than in the case of the neutral oxygen vacancy. The nearest oxygen ions surrounding the vacancy are displaced outwards from the vacant site by about 0.1 – 0.2\AA and the relaxation energy is about 1.4 eV. The formation energy of the neutral zirconium vacancy, determined in the same way as that for the oxygen vacancy, is 24.2 eV. The formation of the zirconium vacancy does not induce any additional states in the band gap—all defect states are located inside the valence band.

Finally, we can combine the results for oxygen interstitials and vacancies, and calculate the formation energies of anion Frenkel defect pairs. For a neutral vacancy-oxygen atom Frenkel pair this energy is about 7.3 eV (with respect to the oxygen atom in the triplet state). This compares well with the results for zircon,¹¹ which also predict 7.3 eV. The energies of charged defect pairs are lower and comprise 6.8 and 5.4 eV for the V^+-O^- and $V^{2+}-O^{2-}$ pairs, respectively. This stems from the lattice polarization which favors charged states and also from the fact the electron affinity of the oxygen interstitial atom/ion is very close or larger than the ionization energy of the neutral/singly charged vacancy (see further discussion in Secs. IV and V). Therefore the electron transfer from a vacancy to an oxygen interstitial is energetically favorable. It is interesting to note that the Frenkel energy for the fully separated pair of doubly charged defects found in our study practically coincides with that predicted using classical pair potentials and the shell model.⁹ However, similar calculations using different interatomic potentials⁸ predict a Frenkel energy of 9.1 eV.

IV. DEFECT LEVELS

In order to study the possible role of defects in photostimulated and thermostimulated processes, and in electronic devices one needs to know the position of defect states with respect to the bottom of the conduction band of zirconia or to other electron or hole sources, such as silicon. In this section we analyze the data obtained for the oxygen and vacancy defects from this perspective.

This analysis requires comparing energies of defects in different charge states. To achieve that we compare total energies of the systems with the same number of electrons. For example, to calculate the vertical ionization energy of the neutral vacancy one can take a difference between the energies of the final state (the sum of the total energies of the perfect crystal with an additional electron and that for the positively charged vacancy with the nuclei positions in the neutral state) and the initial state (the sum of the total energies of the perfect crystal and that for the crystal with the neutral vacancy). The main inaccuracy of this approach is related to the underestimated band gap in our DFT calculations. Below we use the difference

$$\kappa = E_g(\text{exp}) - E_g(\text{theor}), \quad (3)$$

to correct the defect excitation energies, the ionizational potentials and electron affinities. Assuming the experimental value of $E_g(\text{exp}) = 5.4$ eV, this gives $\kappa = 5.4 - 3.19 = 2.21$ eV.

Defining the defect ionizational energy $I_p(D)$ as the vertical excitation energy of an electron from the defect to the bottom of the conduction band, we have

$$I_p(D, q) = E(\text{per}, -) + E(D, q+1) - E(\text{per}, 0) - E(D, q) + \kappa, \quad (4)$$

where $E(\text{per}, -)$ and $E(\text{per}, 0)$ are the calculated energies of the perfect supercell with charge -1 and 0 , respectively, and $E(D, q)$ is the energy of the defect with the charge q (in the elementary charge unit). In Eq. (4) the value $E(D, q+1)$ must be calculated for the geometry of the relaxed defect with the charge q . We can define the electron affinity of the defect $\chi_e(D)$ in exactly the same manner (noting that we now consider an energy gain when the electron from the bottom of the conduction band is trapped at the defect, rather than an excitation energy to be paid) as follows:

$$\chi_e(D, q) = E(\text{per}, -) + E(D, q) - E(\text{per}, 0) - E(D, q-1) + \kappa. \quad (5)$$

Note that the one can consider both “vertical” and “relaxed” electron affinities. In the latter case the lattice relaxation after the electron trapping is included in $E(D, q-1)$. We can also define a hole affinity of the defect $\chi_h(D)$, i.e., the energy gain when a free hole is trapped from the top of the valence band to the defect as follows:

$$\chi_h(D, q) = E(\text{per}, +) + E(D, q) - E(\text{per}, 0) - E(D, q+1). \quad (6)$$

Again, dependent on whether the lattice relaxation in the final state is included or not, one will obtain different affinities. Note that in calculating the hole affinity $\chi_h(D)$, we do not use the correction κ , as we assume that the energy differences between filled states are well reproduced in DFT. From the definitions (5) and (6) it is easy to obtain

$$\chi_h(D, q) + \chi_e(D, q+1) = E_g(\text{exp}). \quad (7)$$

This method is clearly approximate. However, fixing the value of κ allows us to present the results of our calculations in one scale. This scale can be changed if a more “accurate”

TABLE II. Ionizational potential $I_p(D)$, electron $\chi_e(D)$, and hole $\chi_h(D)$ affinities (in eV) of defects in different charge states.

D	V_4^0	V_4^+	V_4^{2+}	O_3^0	O_3^-	O_3^{2-}
$I_p(D)$	3.80	3.98		5.39	5.19	5.19
$\chi_e(D)$		3.33	3.54	3.73	4.62	
$\chi_h(D)$	2.07	1.86		0.07	1.67	0.78

or relevant value for κ will be found. This will require only a shift of our predicted values by a constant.

In further discussion we will consider two types of processes: (i) vertical (Franck-Condon) ionization of defect centers in different charge states into the conduction band and (ii) full (i.e., relaxed) affinities of defect states with respect to electrons from the bottom of the conduction band and holes from the top of the valence band. The calculated values are summarized in Table II and the electron affinities are also shown in a schematic energy diagram in Fig. 7.

We can see that doubly and singly charged vacancies of both types have positive electron affinities for electrons coming from the bottom of the conduction band. The calculated electron affinity for the neutral vacancy is very small and cannot be accurately predicted because the corresponding electron state is lying at the bottom of the conduction band and depends on the accuracy of calculation of the conduction band. The neutral and negatively charged interstitial oxygens also have large electron affinities. The hole affinities for charged oxygen species are large due to the strong defect relaxation. The “vertical” values for these affinities are about 0.2 eV, in line with what one would expect from the DOS and vertical ionization energies.

Yet another relevant issue concerns the electron affinities of these defects with respect to electrons from the bottom of the silicon conduction band at the Si/ZrO₂ interface. This is par-

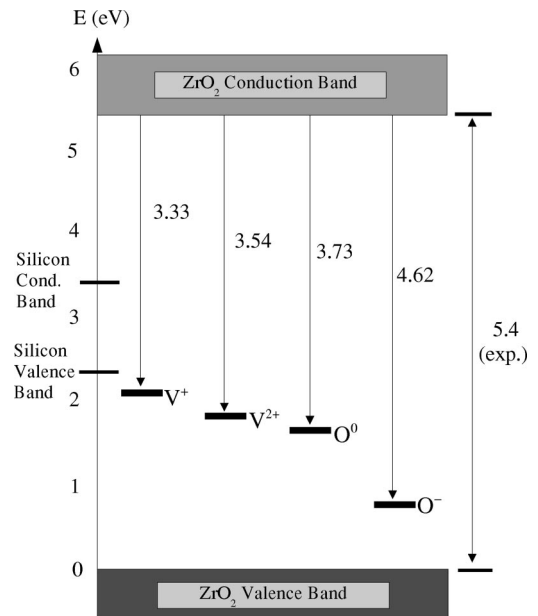


FIG. 7. Energy level diagram showing the electron affinities for various defects in monoclinic zirconia. All energies are in eV.

TABLE III. Defect reactions and associated energies. The values in brackets show the energy difference between the formation energy of the defect pair and the formation energy of the neutral Frenkel pair.

Reaction	Energy (eV)
$O^0 + V^0 \Rightarrow O^- + V^+$	0.5
$O^- + V^+ \Rightarrow O^{2-} + V^{2+}$	1.4
$O^{2-} + O^0 \Rightarrow 2O^-$	-0.9
$V_4^{2+} + V_4^0 \Rightarrow 2V_4^+$	0.2

ticularly relevant for thin oxide films where electrons can tunnel from the interface into defect states.³⁵ Again counting from the top of the valence band (see Fig. 7), we can use the experimental values²² of the valence band offset (2.3 eV) at the interface and the band gap of Si (1.1 eV), and the position of the top of the valence band of ZrO_2 in our calculations to estimate the energy of an electron at the bottom of Si conduction band with respect to the defect levels. As one can see in Fig. 7, doubly and singly charged vacancies, and neutral and singly charged oxygen interstitials can serve as traps for electrons injected from the bottom of the silicon conduction band. Perhaps equally importantly, the top of silicon valence band practically resonates with the neutral oxygen vacancy (see Table II). Therefore these states can serve as shallow traps for holes injected from silicon and participate in hopping hole conductance through oxide.

V. REACTIONS

The above calculations predict the existence of oxygen vacancies and interstitials in different charge states. The number and spatial distribution of defects in each charge state will depend on the method of their creation, presence of the electron source, applied voltage, temperature, and other factors. Assuming a distribution of defects in different charge states and electron transfer between defects, our results allow us to predict the most stable state for each defect pair.

To address this question we compare the total energies for defect pairs in the same total charge state using the total energies of individual defects. The reactions are listed in Table III. Note that we do not include O^+ and V^- defects because we do not treat the results obtained for these defects as reliable enough. As in simple alkali halides, the charge transfer between oxygen vacancies and interstitial atoms is energetically favorable and means that a pair of separated doubly charged defects has about 1.9 eV lower energy than a Frenkel pair of neutral defects.

It is interesting to note that our results predict (see the third reaction in Table III) the decay of two isolated O^- species into the O^{2-} center and a neutral O^0 species. This characteristic is known as “negative U ” behavior. On the other hand, the similar reaction between the two positively charged vacancies (last line in Table III), which was predicted to be an exothermic in yttrium stabilized zirconia,⁴ in our calculations comes out endothermic. This reaction is even less favorable for threefold coordinated vacancy: the energy loss is about 0.4 eV. This discrepancy may result

from the presence of a charged yttrium impurity in the vicinity of the F center in Ref. 4. However, we should note that the repulsion between two positively charged oxygen vacancies at short ($\sim 5 \text{ \AA}$) distances can reverse this very delicate balance.

VI. DISCUSSION

The results of the calculations demonstrate that oxygen interstitials and vacancies in monoclinic zirconia are strongly localized. O_3^0 and O_3^- , V_4^{2+} , and V_4^+ can serve as electron traps and V_4^0 as a shallow hole trap. They have similar structure to analogous defects in cubic oxides. Application of quantum-mechanical methods to study defect states proved to be essential, since ZrO_2 and some of the defect structures are characterized by significant covalent bonding and attempts to model them and the corresponding electrical levels would be impossible in classical shell-model techniques.

However, some of the defect properties cannot be accurately predicted. In particular, the neutral vacancy may have positive electron affinity but it cannot be reliably established in our calculations due to the strong admixture of its electron state at the bottom of the conduction band. This results from two inter-related factors: (i) the band gap is systematically underestimated in plane wave DFT calculations with the PW91 energy functional and (ii) calculations in this method tend to amplify the delocalization of electronic states in shallow energy wells.

The same factors affect the accuracy of our calculation of the optical excitation energy of the neutral oxygen vacancy. We have estimated this energy by the difference of the total energies of the lowest singlet and triplet defect states and obtained 1.2 eV. Since the excited state is very close to the bottom of the conduction band, it is likely that the error is close to that in the value of the band gap, as discussed above. If for rough estimate of the optical absorption energy we increase the calculated value by the same correction $\kappa = 2.21$ eV used to correct the band-gap width, we obtain about 3.4 eV. It is interesting to note that this value is very close to the maximum of the broad band at about 3.4 eV attributed to F centers (neutral vacancies in yttria-stabilized zirconia³⁴).

Our results predict negative U for the O^- center. In other words two O^- centers are unstable with respect to disproportionation into O^{2-} and O^0 centers. They also predict stability of V^+ centers with respect to disproportionation into V^{2+} and V^0 . The calculated reaction energies can be affected by several factors. One is the Coulomb interaction between a charged defect and its periodic images in the total energy calculation for each such defect. It is included in calculations of electron affinities, ionization energies and electron transfer reactions using the technique described in Refs. 23,24. For a well-localized single charged defect this correction is only ~ 0.1 eV due to the large size of the supercell ($\sim 10 \text{ \AA}$) and the large static dielectric constant of the material ($\epsilon \sim 25^5$). However, the dielectric constant of zirconia is not well defined and will be certainly different in thin zirconia films on silicon. Nevertheless, the large size of our unit cell means that this uncertainty should not affect our qualitative conclu-

sions. Another factor is the Coulomb interaction between charged defects in each defect pair in Table III. In our calculations this interaction is neglected. At short (less than ~ 10 Å) distances between charged defects it can affect our predictions. Yet another factor is polarization of silicon by charged defects (image interaction), which can affect both the defect formation energies and charge transfer reactions. These effects should be studied in more detail for particular cases.

The predicted possibility of electron transfer from silicon into oxygen vacancies and interstitials may have different consequences for the growth and properties of zirconia films on silicon. In particular, the electron transfer from silicon onto interstitial oxygen atoms will create charged oxygen ions, which will become attracted to the interface by the image interaction with silicon. This may affect diffusion of these species and thus the kinetics of oxide growth. This problem certainly requires a more detailed study, including the mechanism of diffusion of oxygen species in zirconia.

Another issue concerns the role of defect species in oxide charging and leakage current. The predicted electron affinities of charged vacancies suggest that they can be neutralized and will not facilitate oxide charging. However, if the neutral vacancy can trap an extra electron in a shallow state, it can serve as a transient state for an electron transfer through

oxide and thus will contribute to leakage current. Therefore this problem also requires further study.

Our results also allow us to make some conclusions concerning radiation stability of oxide. The anion Frenkel energies predicted in our calculations are all larger than the band gap. Therefore Frenkel pairs cannot be formed as a result of recombination of electron-hole pairs created by electron or photon irradiation. This suggests that the excitonic mechanism of radiation damage which is extremely effective in alkali halides and in some oxides³⁶ is most certainly ineffective in zirconia. This result agrees with the well-known radiation stability of zirconia.

ACKNOWLEDGMENTS

The authors wish to thank V. Afanas'ev, M. Hakala, A. Korkin, N. Petrik, A. M. Stoneham, and A. M. Szymanski for useful discussions. We are grateful to L. N. Kantorovich, A. A. Sokol, and P. V. Sushko for very useful critical comments on the manuscript. A.S.F. wishes to thank the Center for Scientific Computing, Helsinki for use of its computational resources. We are grateful to EPSRC and Fujitsu for financial support of this work. The LEV00 code²⁹ was used for calculation of density maps and DOS.

-
- ¹E. Ryskhewitch and D. W. Richerson, *Oxide Ceramics. Physical Chemistry and Technology* (Academic, Orlando, 1985).
- ²C. J. Howard, R. J. Hill, and B. E. Reichert, *Acta Crystallogr., Sect. B: Struct. Sci.* **44**, 116 (1988).
- ³E. V. Stefanovich, A. L. Shluger, and C. R. A. Catlow, *Phys. Rev. B* **49**, 11 560 (1994).
- ⁴G. Stapper, M. Bernasconi, N. Nicoloso, and M. Parrinello, *Phys. Rev. B* **59**, 797 (1999).
- ⁵A. I. Kingon, J. P. Maria, and S. K. Streiffer, *Nature (London)* **406**, 1032 (2000).
- ⁶T. S. Jeon, J. M. White, and D. L. Kwong, *Appl. Phys. Lett.* **78**, 368 (2001).
- ⁷M. Copel, M. Gribelyuk, and E. Gusev, *Appl. Phys. Lett.* **76**, 436 (2000).
- ⁸W. C. Mackrodt and P. M. Woodrow, *J. Am. Ceram. Soc.* **69**, 277 (1986).
- ⁹A. Dwivedi and A. N. Cormack, *Philos. Mag. A* **61**, 1 (1990).
- ¹⁰B. Králik, E. K. Chang, and S. G. Louie, *Phys. Rev. B* **57**, 7027 (1998).
- ¹¹J. P. Crocombette, *Phys. Chem. Miner.* **27**, 138 (1999).
- ¹²G. Kresse and J. Furthmüller, *Comput. Mater. Sci.* **6**, 15 (1996).
- ¹³G. Kresse and J. Furthmüller, *Phys. Rev. B* **54**, 11 169 (1996).
- ¹⁴J. P. Perdew, J. A. Chevary, S. H. Vosko, K. A. Jackson, M. R. Pederson, D. J. Singh, and C. Fiolhais, *Phys. Rev. B* **46**, 6671 (1992).
- ¹⁵D. Vanderbilt, *Phys. Rev. B* **41**, 7892 (1990).
- ¹⁶G. Kresse and J. Hafner, *J. Phys.: Condens. Matter* **6**, 8245 (1994).
- ¹⁷D. Murnaghan, *Proc. Natl. Acad. Sci. U.S.A.* **30**, 244 (1944).
- ¹⁸G. Jomard, T. Petit, A. Pasturel, L. Magaud, G. Kresse, and J. Hafner, *Phys. Rev. B* **59**, 4044 (1999).
- ¹⁹S. T. Pantelides, D. J. Mickish, and A. B. Kunz, *Phys. Rev. B* **10**, 5203 (1974).
- ²⁰R. H. French, S. J. Glass, F. S. Ohuchi, Y. N. Xu, and W. Y. Ching, *Phys. Rev. B* **49**, 5133 (1994).
- ²¹D. W. McComb, *Phys. Rev. B* **54**, 7094 (1996).
- ²²M. Houssa, M. Tuominen, M. Naili, V. Afanas'ev, A. Stesmans, S. Haukka, and M. M. Heyns, *Appl. Phys.* **87**, 8615 (2000).
- ²³M. Leslie and M. J. Gillan, *J. Phys. C* **18**, 973 (1985).
- ²⁴L. N. Kantorovich, *Phys. Rev. B* **60**, 15 476 (1999).
- ²⁵A. M. Stoneham, M. A. Szymanski, and A. L. Shluger, *Phys. Rev. B* **63**, R241304, (2001).
- ²⁶M. A. Szymanski, A. L. Shluger, and A. M. Stoneham, *Phys. Rev. B* **63**, 224207 (2001).
- ²⁷D. R. Hamann, *Phys. Rev. Lett.* **81**, 3447 (1998).
- ²⁸G. Pacchioni, and G. Ieranó, *Phys. Rev. B* **56**, 7304 (1997).
- ²⁹L. N. Kantorovich, www.cmmmp.ucl.ac.uk/~lev/codes/lev00/index.html (unpublished) (1996–2001).
- ³⁰J. Laegsgaard and K. Stokbro, *Phys. Rev. Lett.* **86**, 2834 (2001).
- ³¹V. Sulimov, S. Casassa, C. Pisani, J. Garapon, and B. Poumellec, *Modell. Simul. Mater. Sci. Eng.* **8**, 763 (2000).
- ³²E. Scorza, U. Birkenheuer, and C. Pisani, *J. Chem. Phys.* **107**, 9645 (1997).
- ³³A. L. Shluger and K. Tanimura, *Phys. Rev. B* **61**, 5392 (2000).

- ³⁴D. Nagle, V. R. Paivernerker, A. N. Petelin, and G. Groff, *Mater. Res. Bull.* **24**, 619 (1989).
- ³⁵W. B. Fowler, J. K. Rudra, M. E. Zvanut, and F. J. Feigl, *Phys. Rev. B* **41**, 8313 (1990).
- ³⁶K. S. Song and R. T. Williams, *Self-Trapped Excitons* (Springer-Verlag, Berlin, 1993).
- ³⁷P. Aldebert and J. P. Traverse, *J. Am. Ceram. Soc.* **68**, 34 (1985).
- ³⁸C. J. Howard, R. J. Hill, and B. E. Reichert, *Acta Crystallogr., Sect. B: Struct. Sci.* **44**, 116 (1988).